Theor Chem Acc (2009) 124:409–420
DOI 10.1007/s00214-009-0631-z

REGULAR ARTICLE

Theoretical study on the ion–molecule reaction of HCN^+ with NH_3

Yan Li · Hui-ling Liu · Yan-bo Sun · Zhuo Li · Xu-ri Huang · Chia-chung Sun

Received: 28 June 2009 / Accepted: 28 August 2009 / Published online: 19 September 2009

Abstract A detailed theoretical study is carried out at the B3LYP/6-311G(d,p) and CCSD(T)/6-311++G(3df,2pd) (single-point) levels as an attempt to investigate the mechanism of the little understand ion–molecule reaction between HCN^+ and NH_3. Various possible reaction pathways are considered. It is shown that six dissociation products $\mathbf{P_1}(NH_3^+ + HCN)$, $\mathbf{P_2}(NH_4^+ + CN)$, $\mathbf{P_3}(NH_3^+ + HNC)$, $\mathbf{P_9}(HCNH^+ + NH_2)$ $\mathbf{P_{10}}(NCNH_3^+ + H)$, and $\mathbf{P_{12}}(HNCNH_2^+ + H)$ are both thermodynamically and kinetically feasible. Among these products, $\mathbf{P_1}$ is the most competitive product with predominant abundance. $\mathbf{P_3}$ and $\mathbf{P_9}$ may be the second feasible products with comparable yields. $\mathbf{P_{12}}$ may be the least possible product followed by the almost negligible $\mathbf{P_2}$ and $\mathbf{P_{10}}$. Because the isomers and transition states involved in the $HCN^+ + NH_3$ reaction all lie below the reactant, the title reaction is expected to be rapid, which is consistent with the measured large rate constant in experiment. The title reaction may have a potential relevance in Titan's atmosphere, where the temperature is very low. Furthermore, our calculated results are compared with the previous experimental findings.

Keywords Reaction mechanism · Potential energy surface (PES) · HCN^+ · NH_3

Electronic supplementary material The online version of this article (doi:10.1007/s00214-009-0631-z) contains supplementary material, which is available to authorized users.

Y. Li · H. Liu · Y. Sun · Z. Li · X. Huang (✉) · C. Sun
State Key Laboratory of Theoretical and Computational Chemistry, Institute of Theoretical Chemistry, Jilin University, 130023 Changchun, People's Republic of China
e-mail: snow2007liyan@163.com

1 Introduction

Titan, the largest satellite of Saturn, has received considerable attention due to its unique atmosphere. The structure and composition of Titan's atmosphere has long been the subject of extensive studies [1–6]. It is shown that Titan's dense and composed atmosphere is mainly made of nitrogen (N_2) and methane (CH_4), but also contains traces of hydrogen, ethane (C_2H_6), ethylene (C_2H_4), acetylene (C_2H_2), hydrogen cyanide (HCN), acetonitrile (CH_3CN), cyanoacetylene (HC_3N) and cyanogen (C_2N_2) [7–11]. Solar radiation and magnetospheric electrons ionize Titan's major constitutes, N_2 and CH_4 to generate the primary ions N^+, N_2^+, CH^+, CH_2^+, CH_3^+, and CH_4^+ [12–16]. Subsequently, these ions can react further with other neutral species that is present in Titan's atmosphere. Such ion-neutral reactions generally take place very fast and may thus play a crucial role in depleting old molecules or ions and synthesizing new molecule or ions. Until now, a large number of investigations have been performed to model the ion-neutral reactions which take place in Titan's atmosphere [17–24].

Among these studies, the reaction of HCN^+ with NH_3 attracts our great interest. However, to the best of our knowledge, only one experimental study has been carried out. The measured rate constant at room temperature is 2.8×10^{-9} cm^3 s^{-1} [17]. Moreover, McEwan et al. [17] proposed three channels for the reaction of HCN^+ with NH_3 as:

$$\begin{aligned} HCN^+ + NH_3 &\rightarrow NH_3^+ + HCN \ 0.6 \\ &\rightarrow NH_4^+ + CN \ 0.05 \\ &\rightarrow HCNH^+ + NH_2 \ 0.3 \end{aligned}$$

Unfortunately, no theoretical study has been reported until now. Without detailed potential energy surface (PES)

information, it is difficult to discuss the mechanism of the title reaction. Therefore, in the present paper, we performed a detailed theoretical study on the reaction of HCN^+ with NH_3. Our main goal is to provide elaborated isomerization and dissociation pathways of the title reaction and thereby to interpret previous experimental observations.

2 Computational methods

All calculations are carried out using the GUASSIAN 98 program package [25]. The optimized geometries and harmonic frequencies of the reactant, products, isomers and transition states are calculated at the B3LYP/6-311G(d,p) level. To confirm the connections of the transition states between designated isomers, we performed intrinsic reaction coordinate (IRC) calculations at the same level of theory. Furthermore, to yield more reliable energetic data, single-point calculations are performed at the CCSD(T)/6-311++G(3df,2pd) level using the B3LYP/6-311G(d,p)-optimized geometries. To test the reliability of the results, we performed additional single-point energy calculations for some critical species at the G3B3 level using the B3LYP/6-311G(d,p)-optimized geometries and scaled B3LYP/6-311G(d,p)-zero-point energies.

3 Results and discussion

The optimized structures of reactant and products are shown in Fig. 1, while the optimized structures of isomers and transition states are depicted in Figs. 2 and 3, respectively. For simplicity, only the calculated $\triangle E$, $\triangle H$, $\triangle S$, and $\triangle G$ of the reactant, products, isomers and transition states are shown in Table 1. The other informations are available in supporting materials. For convenient discussion, the total energy of the reactant R ($HCN^+ + NH_3$) is set as zero for reference. The symbol TSm/n is used to denote the transition state connecting isomers m and n. By means of the interrelationship among the reactant, products, isomers and transition states, the schematic potential energy surface (PES) of the $HCN^+ + NH_3$ reaction is presented in Fig. 4. Unless otherwise specified, the CCSD(T)/6-311++G(3df,2pd)//B3LYP/6-311G(d,p) + ZPVE energies are used throughout.

3.1 Initial association

HCN^+ has $C_{\infty v}$ symmetry and $^2\sum$ electronic state. The respective spin distribution of HCN^+ is −0.013712, 0.419415, and 0.594297e on H, C, and N. So, both C and N can be viewed as the active site of HCN^+. On the other hand, at the B3LYP/6-311G(d,p) level, the HOMO and LUMO energies of HCN^+ are −0.74452 and −0.62122 a.u., respectively, while those of NH_3 are −0.25848 and 0.03901 a.u., respectively. The absolute energy difference 0.36274 a.u. between $E(HOMO_{NH3})$ and $E(LUMO^+_{HCN})$ is smaller than 0.78353 a.u. between $E(HOMO^+_{HCN})$ and $E(LUMO_{NH3})$. Therefore, according to frontier orbital theory, the interaction should take place between HCN^+'s LUMO and NH_3's HOMO resulting in two initial adducts **1** $HCNNH_3^+$ (−86.9) and **2** $NCHNH_3^+$ (−110.1). Values in parentheses are relative energies in kcal/mol with reference to the reactant R ($HCN^+ + NH_3$)(0.0). The HOMO and LUMO of HCN^+ and NH_3 are shown in Fig. 5.

With the large heat released from the initial step, isomers **1** and **2** can take further changes. For convenient discussion, the evolution pathways of **1** are shown in Fig. 4a while those of **2** are shown in Fig. 4b.

3.2 Reaction pathways

3.2.1 Reaction pathways of 1

Starting from **1**, nine kinds of dissociation products $\mathbf{P_1}(NH_3^+ + HCN)$, $\mathbf{P_2}(NH_4^+ + CN)$, $\mathbf{P_3}(NH_3^+ + HNC)$, $\mathbf{P_4}(HCNNH_2^+ + H)$, $\mathbf{P_5}$(c-$NHNCH_2^+ + H$), $\mathbf{P_6}$(c-CHN $NH_2^+ + H$), $\mathbf{P_7}(HNNCH_2^+ + H)$, $\mathbf{P_8}(HCNNH^+ + H_2)$, and $\mathbf{P_9}(HCNH^+ + NH_2)$ can be obtained as shown in Fig. 4a. In the following part, we will discuss the formation pathways of these nine products.

$$\mathbf{P_1}\left(\mathbf{NH_3^+ + HCN}\right) \quad (1)$$

From Fig. 4a, we find that two pathways are energetically possible to form the charge-transfer product $\mathbf{P_1}$. They can be written as:

Path $\mathbf{P_1}$ **(1)** $\quad \mathbf{R \rightarrow 1 \rightarrow 3 \rightarrow P_1}$

Path $\mathbf{P_1}$ **(2)** $\quad \mathbf{R \rightarrow 1 \rightarrow 6a \rightarrow 6b \rightarrow 7 \rightarrow P_1}$

1 $HCNNH_3^+$ can undergo N–N bond rupture to form the weakly bound complex **3** $HCN\cdots NH_3^+$ before the final product $\mathbf{P_1}$ as in **path** $\mathbf{P_1}$**(1)**. Alternatively, **1** can take 2,3-H-shift to generate **6a** $HCNHNH_2^+$, which can convert to **6b** via internal C–N bond rotation. Then, **6b** undergoes concerted N–N bond rupture along with H-shift to form the weakly bound complex **7** $HCN\cdots HNH_2^+$. Finally **7** can directly dissociate to $\mathbf{P_1}$ as in **path** $\mathbf{P_1}$**(2)**. It should be noted that the step of **7**→$\mathbf{P_1}$ is a barrierless process as confirmed by the pointwise potential curve calculated at the B3LYP/6-311G(d,p) level (shown in Fig. 6a).

Clearly, **path** $\mathbf{P_1}$**(1)** is simpler than **path** $\mathbf{P_1}$**(2)**. Most importantly, the energy barrier 0.2(**1**→**3**) kcal/mol involved in **path** $\mathbf{P_1}$**(1)** is significantly lower than 54.6

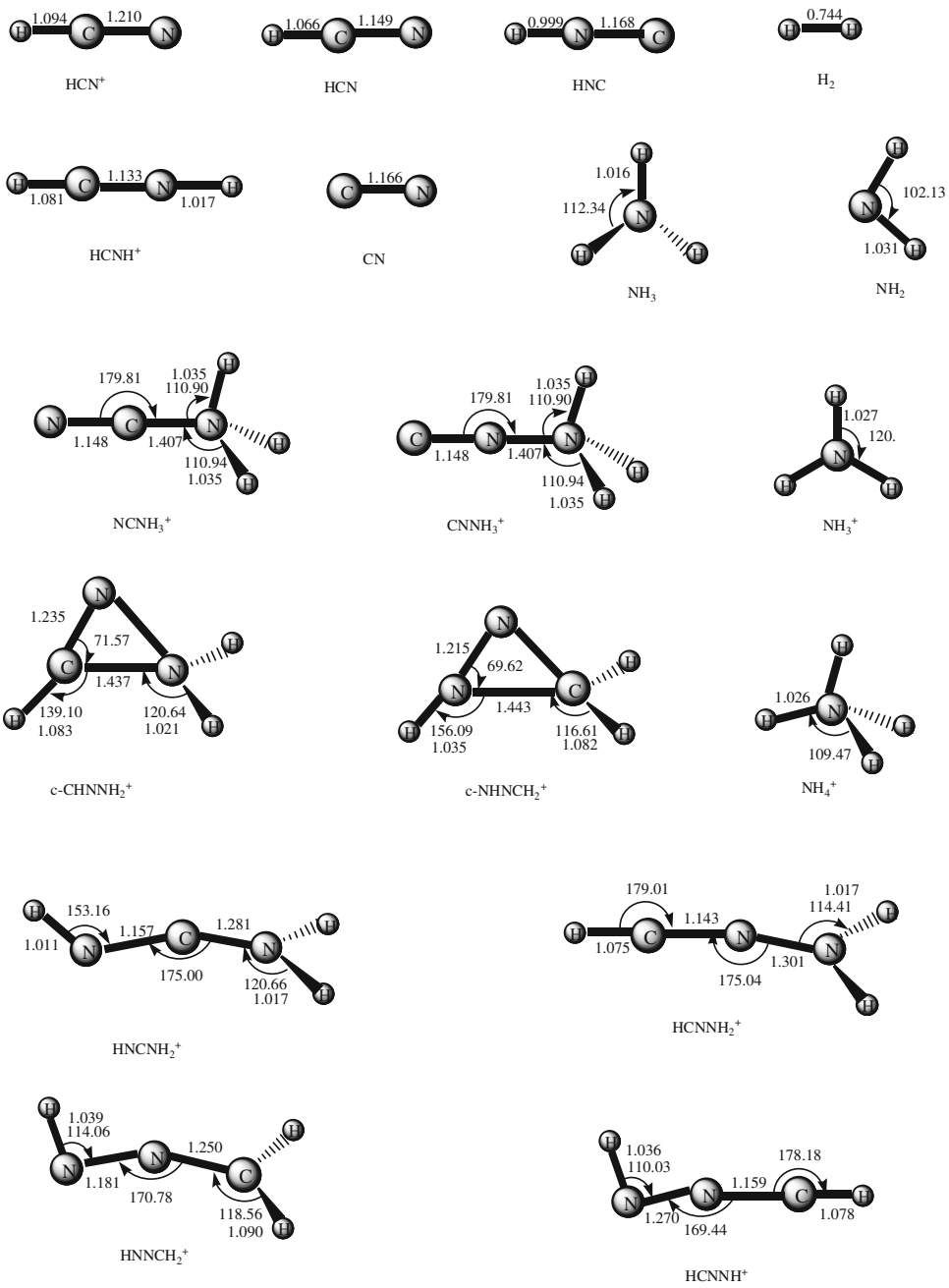

Fig. 1 The optimized structures of the reactant and products at the B3LYP/6-311G(d,p) level. Distances are given in angstroms and angles in degrees

(**1→6a**), 7.0 (**6a→6b**) and 13.6 (**6b→7**) kcal/mol in **path $P_1(2)$**. Thus, we expect that **path $P_1(1)$** is the optimal channel to form $\mathbf{P_1}$.

$$\mathbf{P_2}\left(\mathbf{NH_4^+ + CN}\right) \text{ and } \mathbf{P_3}\left(\mathbf{NH_3^+ + HNC}\right) \quad (2)$$

The formation pathway of **3** $HCN\cdots NH_3^+$ is the same as that in **path $P_1(1)$**. Then **3** can undergo either H-shift along with N–N bond fission to yield $\mathbf{P_2}$ or 1,2-H-shift accompanied by N–N bond fission to generate $\mathbf{P_3}$. The barriers for **3→P_2** and **3→P_3** conversions are 43.7 and 54.3 kcal/mol, respectively. The formation pathway of $\mathbf{P_2}$ and $\mathbf{P_3}$ can be depicted as:

$$\mathbf{Path\,P_2\,R \rightarrow 1 \rightarrow 3 \rightarrow P_2}$$

$$\mathbf{Path\,P_3\,R \rightarrow 1 \rightarrow 3 \rightarrow P_3}$$

$$\mathbf{P_4}\,(\mathbf{HCNNH_2^+ + H}) \quad (3)$$

There are two pathways to form product $\mathbf{P_4}$ which can be listed as:

$$\mathbf{Path\,P_4\,(1)\,R \rightarrow 1 \rightarrow P_4}$$

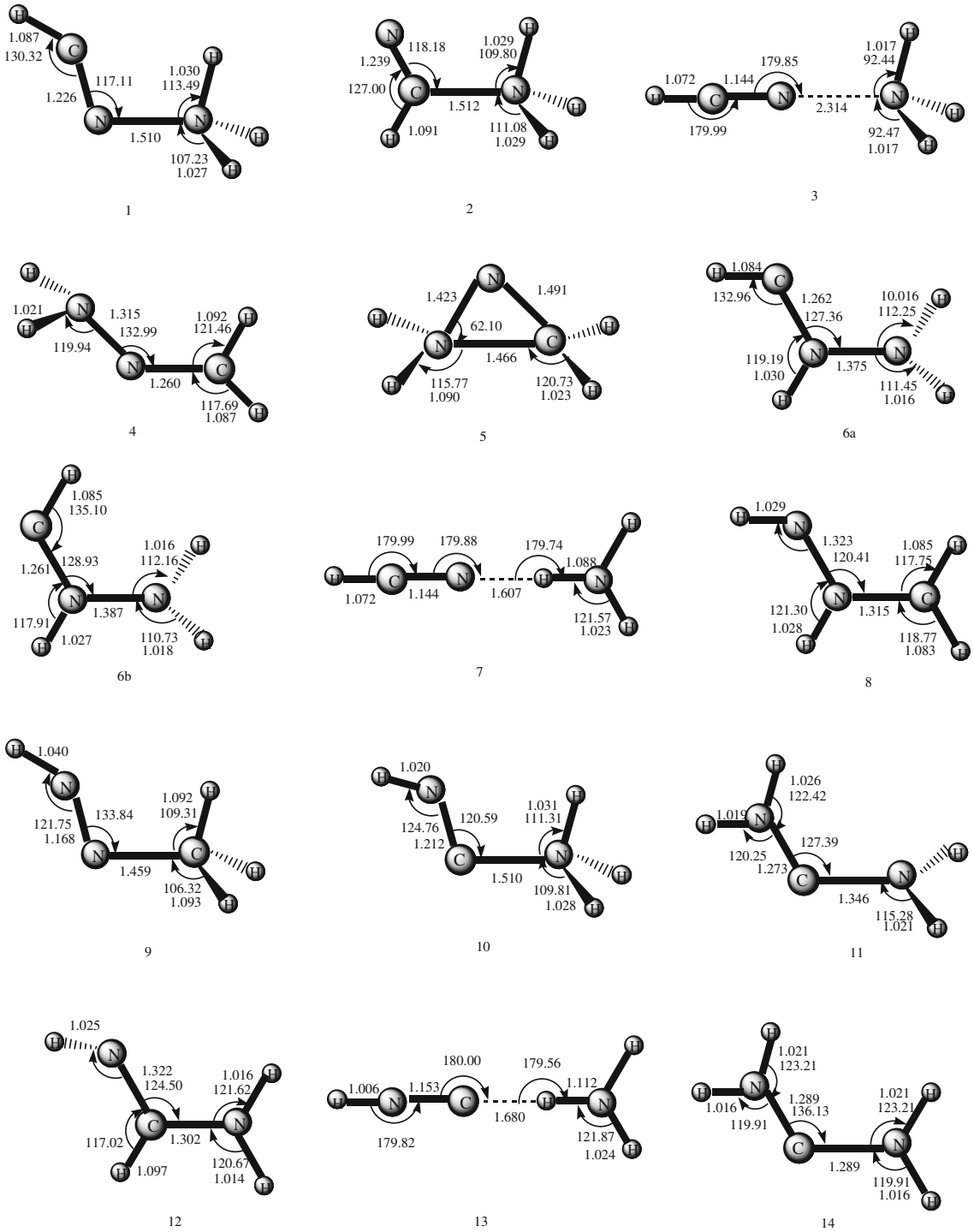

Fig. 2 The optimized structures of the isomers at the B3LYP/6-311G(d,p) level. Distances are given in angstroms and angles in degrees

Path $\mathbf{P_4}$ (2) $\mathbf{R \rightarrow 1 \rightarrow 4 \rightarrow P_4}$

1 $HCNNH_3^+$ can take either H-elimination to form $\mathbf{P_4}$ as in **path $\mathbf{P_4}$(1)** or continuously 1,3-H-shift and C–H bond cleavage to form **4** $CH_2NNH_2^+$, then to $\mathbf{P_4}$ as in **path $\mathbf{P_4}$(2)**. In **path $\mathbf{P_4}$(1)**, only one barrier 50.3 kcal/mol is needed to climbed from **1** to $\mathbf{P_4}$, while in **path $\mathbf{P_4}$(2)**, two barriers are needed to surmount, those are 46.7 and 54.3 kcal/mol for the steps of **1**→**4** and **4**→$\mathbf{P_4}$, respectively. Therefore, the optimal channel to form $\mathbf{P_4}$ is **path $\mathbf{P_4}$(1)**.

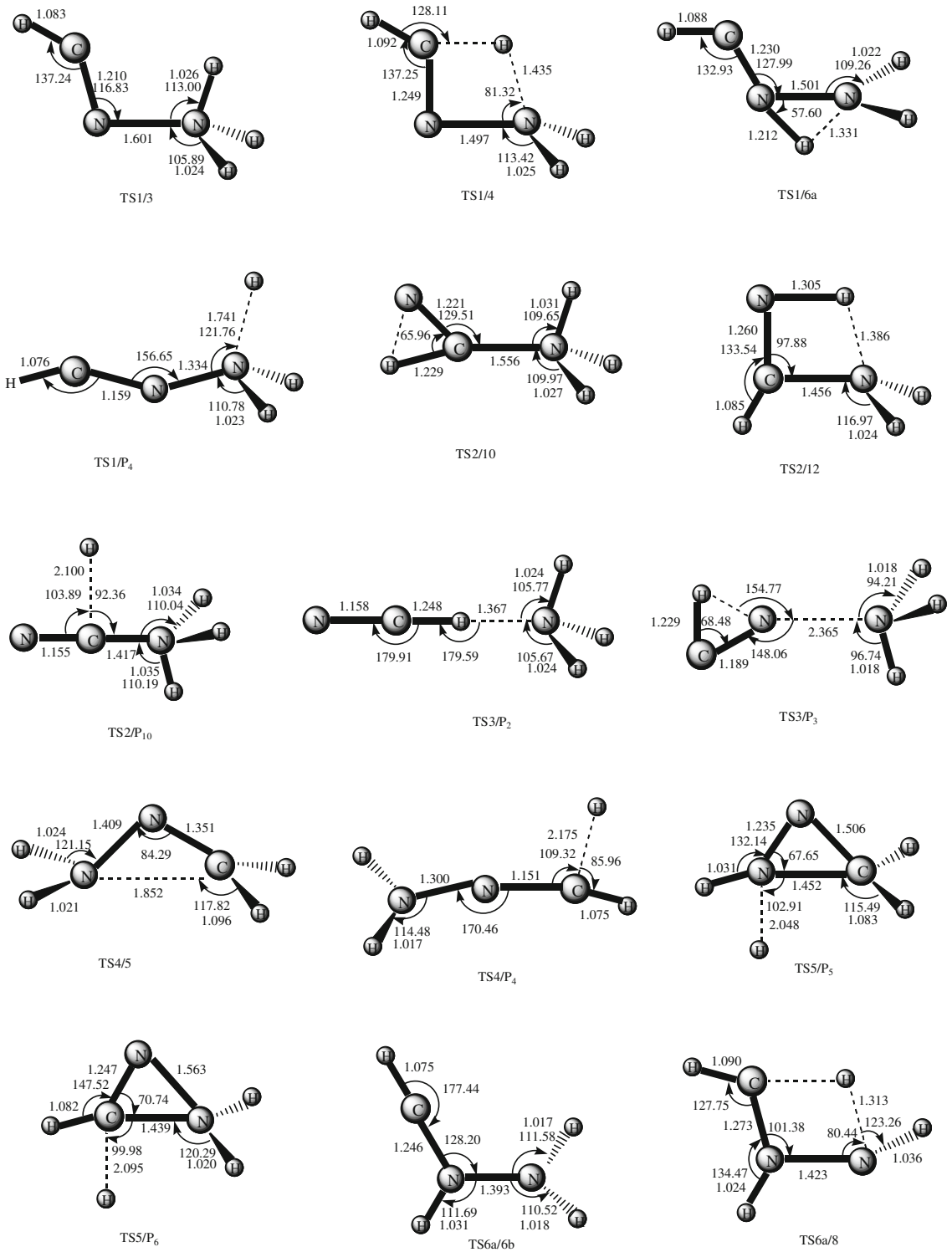

Fig. 3 The optimized structures of the transition states at the B3LYP/6-311G(d,p) level. Distances are given in angstroms and angles in degrees

$$\mathbf{P_5}\,(\mathbf{c\text{-}NHNCH_2^+ + H}) \text{ and } \mathbf{P_6}(\mathbf{c\text{-}CHNNH_2^+ + H}) \qquad (4)$$

Only one feasible pathway is associated with formation of either $\mathbf{P_5}$ or $\mathbf{P_6}$. They can be written as:

Path $\mathbf{P_5}$ $\mathbf{R \rightarrow 1 \rightarrow 4 \rightarrow 5 \rightarrow P_5}$

Path $\mathbf{P_6}$ $\mathbf{R \rightarrow 1 \rightarrow 4 \rightarrow 5 \rightarrow P_6}$

4 $CH_2NNH_2^+$ undergoes a ring-closure process to generate the three-membered cyclic isomer **5** c-$CH_2NNH_2^+$. Subsequently, **5** can undergo either N–H bond rupture lead to $\mathbf{P_5}$ or C–H bond cleavage lead to $\mathbf{P_6}$. The energy

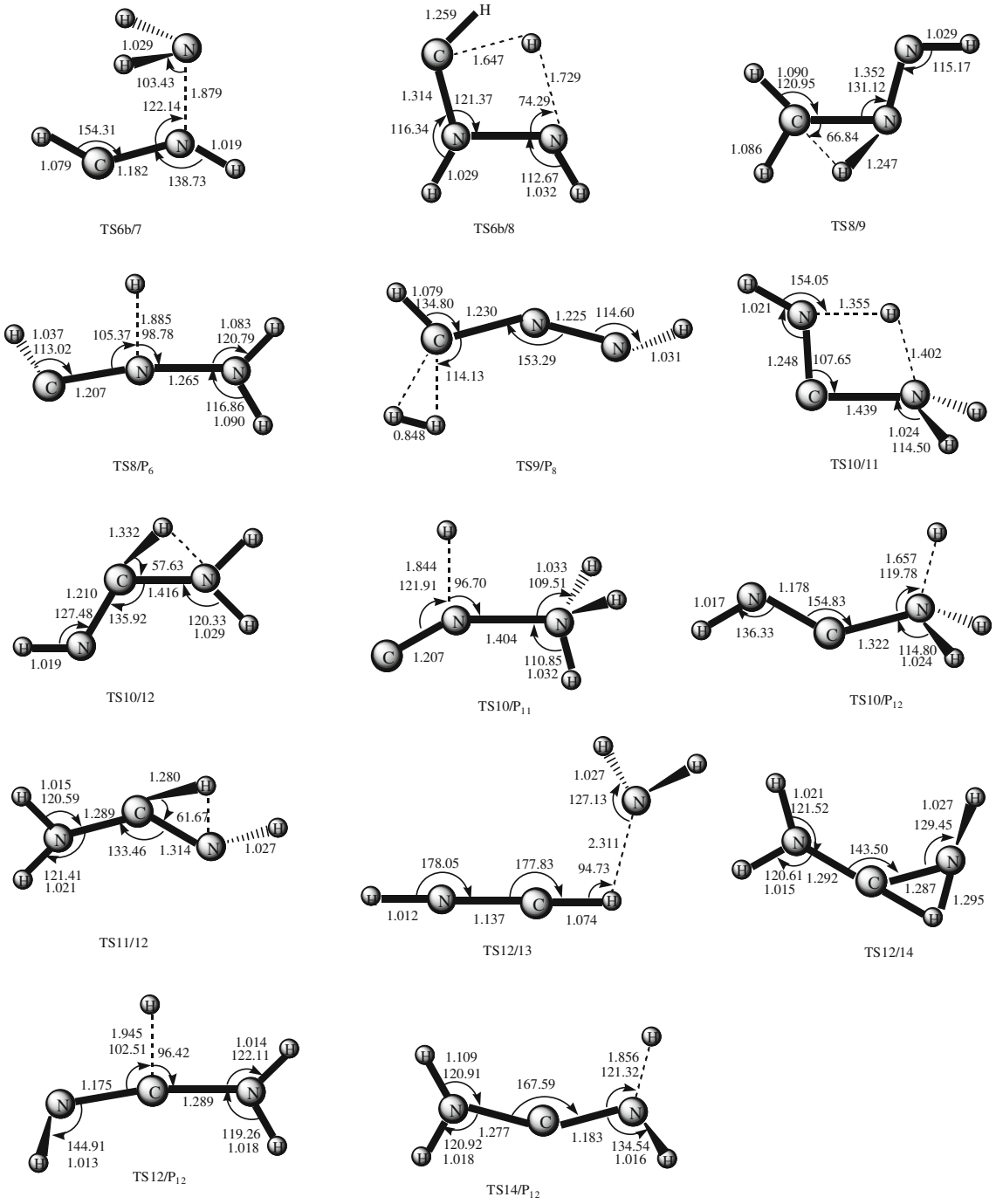

Fig. 3 continued

barriers for **4→5**, **5→P5** and **5→P6** conversions are 48.1, 64.8 and 49.6 kcal/mol, respectively.

$$\mathbf{P_7}\ (\mathbf{HNNCH_2^+ + H}) \tag{5}$$

From Fig. 4a, we find that two pathways are energetically possible to form **P7** which can be presented as:

Path P7 (1) R → 1 → 6a → 8 → P7

Path P7 (2) R → 1 → 6a → 6b → 8 → P7

The formation of **6** (**6a**, **6b**) $HCNHNH_2^+$ is the same as that in **path P1(2)**. Subsequently, both **6a** and **6b** can take 1,3-H-shift which gives rise to **8** $HNNHCH_2^+$. Finally, **8** undergoes internal N–H bond rupture lead to **P7**.

Path P7(1) is slightly simple than **path P7(2)**, thus we expect **path P7(1)** is the favorite channel to generate **P7**.

Table 1 Relative energies(*E*), enthalpies(*H*), Gibbs free energies (*G*) in kcal/mol and entropies (*S*) in calmol^{-} K^{-1} of the reactant, products, isomers and transition states for the HCN^{+}+NH_3 reaction

Species	*E*	*H*	*S*	*G*
Reactant	0.0	0.0	0.0	0.0
$P_1(NH_3^+ + HCN)$	−91.9	−91.9	−0.3	−91.8
$P_2(NH_4^+ + CN)$	−88.8	−89.0	−3.1	−88.1
$P_3(NH_3^+ + HNC)$	–77.9	–77.7	0.6	–77.9
$P_4(HCNNH_2^+ + H)$	−49.4	−49.5	−8.0	−47.1
P_5(c-$NHNCH_2^+ + H$)	−19.6	−20.1	−9.5	−17.3
P_6(c-$CHNNH_2^+ + H$)	−33.2	−33.8	−9.4	−31.0
$P_7(HNNCH_2^+ + H)$	−41.0	−41.4	−8.8	−38.8
$P_8(HCNNH^+ + H_2)$	−48.7	−48.4	−4.5	−47.0
$P_9(HCNH^+ + NH_2)$	−76.1	−76.1	−0.2	−76.0
$P_{10}(NCNH_3^+ + H)$	−61.9	−62.2	−8.0	−59.8
$P_{11}(CNNH_3^+ + H)$	−23.4	−23.4	−5.4	−21.8
$P_{12}(HNCNH_2^+ + H)$	−87.5	−87.6	−7.4	−85.4
1	−86.9	−88.3	−30.9	−79.1
2	−110.1	−111.7	−31.8	−102.2
3	−110.9	−111.5	−24.8	−104.1
4	−100.9	−102.4	−31.9	−92.9
5	−79.5	−81.5	−34.9	−71.1
6a	−75.9	−77.6	−32.9	−67.8
6b	−75.5	−77.1	−32.6	−67.4
7	−115.9	−116.7	−26.4	−108.8
8	−95.3	−97.2	−34.1	−87.1
9	−96.5	−98.0	−31.7	−88.6
10	−110.9	−112.4	−31.4	−103.1
11	−118.8	−120.7	−34.3	−110.5
12	−121.0	−122.7	−33.1	−112.9
13	−102.5	−103.2	−26.1	−95.4
14	−128.4	−130.0	−32.5	−120.3
TS1/3	−86.7	−88.2	−30.8	−79.0
TS1/4	−40.2	−42.1	−34.1	−31.9
TS1/6a	−32.3	−33.9	−31.7	−24.4
$TS1/P_4$	−36.6	−37.9	−30.6	−28.7
TS2/10	−68.2	−69.4	−29.6	−60.6
TS2/12	−75.3	−77.3	−34.5	−67.0
$TS2/P_{10}$	−58.4	−59.6	−29.2	−50.9
$TS3/P_2$	−67.2	−68.2	−27.7	−60.0
$TS3/P_3$	−56.6	−56.7	−16.7	−51.7
TS4/5	−52.8	−54.8	−34.4	−44.5
$TS4/P_4$	−46.6	−47.5	−27.7	−39.2
$TS5/P_5$	−14.7	−16.3	−32.6	−6.6
$TS5/P_6$	−29.9	−31.5	−32.3	−21.9
TS6a/6b	−68.9	−70.6	−32.9	−60.8
TS6a/8	−39.6	−41.4	−33.9	−31.4
TS6b/7	−61.9	−63.2	−29.4	−54.4
TS6b/8	−1.2	−2.9	−33.1	7.0
TS8/9	−40.8	−42.7	−34.2	−32.5
$TS8/P_7$	−29.2	−49.6	−32.0	−21.2
$TS9/P_8$	−24.4	−25.9	−32.0	−16.3
TS10/11	−71.2	−73.1	−34.2	−62.9
TS10/12	−63.1	−64.7	−33.0	−54.9
$TS10/P_{11}$	−14.7	−15.8	−27.4	−7.6
$TS10/P_{12}$	−69.3	−70.9	−32.4	−61.2
TS11/12	−76.3	−78.0	−33.7	−68.0
TS12/13	−89.3	−90.1	−25.5	−82.5
TS12/14	−74.0	−75.5	−32.1	−65.9
$TS12/P_{12}$	−80.7	−81.9	−30.2	−72.9
$TS14/P_{12}$	−78.8	−71.5	−30.7	−62.4

The energy barriers for **1→6a**, **6a→8**, and **8→P$_7$** conversions are 54.6, 36.3, and 66.1 kcal/mol, respectively.

P$_8$ (HCNNH$^+$ + H$_2$) (6)

There are two feasible pathways to form **P$_8$** which can be written as:

Path P$_8$ (1) R → 1 → 6a → 8 → 9 → P$_8$

Path P$_8$ (2) R → 1 → 6a → 6b → 8 → 9 → P$_8$

Besides dissociate to **P$_7$**, **8** $HNNHCH_2^+$ can also isomerizes to **9** $HNNCH_3^+$ via a 1,2-H-shift process. Finally, **9** undergoes H_2-elimination lead to **P$_8$** as in **path P$_8$(1)** and **path P$_8$(2)**. The energy barriers for the steps of **8→9** and **9→P$_8$** are 54.5 and 72.1 kcal/mol, respectively. By comparison, we expect **path P$_8$(1)** is competitive than **path P$_8$(2)**.

P$_9$ (HCNH$^+$ + NH$_2$) (7)

As seen from Fig. 4a, only one pathway is associated with the formation of **P$_9$**. It can be written as:

Path P$_9$ R → 1 → 6a → 6b → 7 → P$_9$

The formation pathway of **7** $HCN\cdots HNH_2^+$ has been discussed previously. Subsequently, **7** can directly dissociate to **P$_9$** without any encounter barrier. To further confirm **7→P$_9$** is a barrierless process, we calculate the pointwise potential curve at the B3LYP/6-311G(d,p) level. The dissociation curve of **7** is shown in Fig. 6b.

As shown in Fig. 4a, two products **P$_1$**(NH_3^++HCN) and **P$_9$**($HCNH^+$+NH_2) can be formed via **7**. However, **P$_9$**(−76.1) is much higher than **P$_1$**(−91.9). Thus, **P$_1$** should be the dominant product from **7**, **path P$_9$** may have negligible contribution to the title reaction.

3.2.2 *Reaction pathways of 2*

Starting from **2**, five kinds of dissociation products **P$_3$**(NH_3^++HNC), **P$_9$**($HCNH^+$+NH_2), **P$_{10}$**($NCNH_3^+$+H),

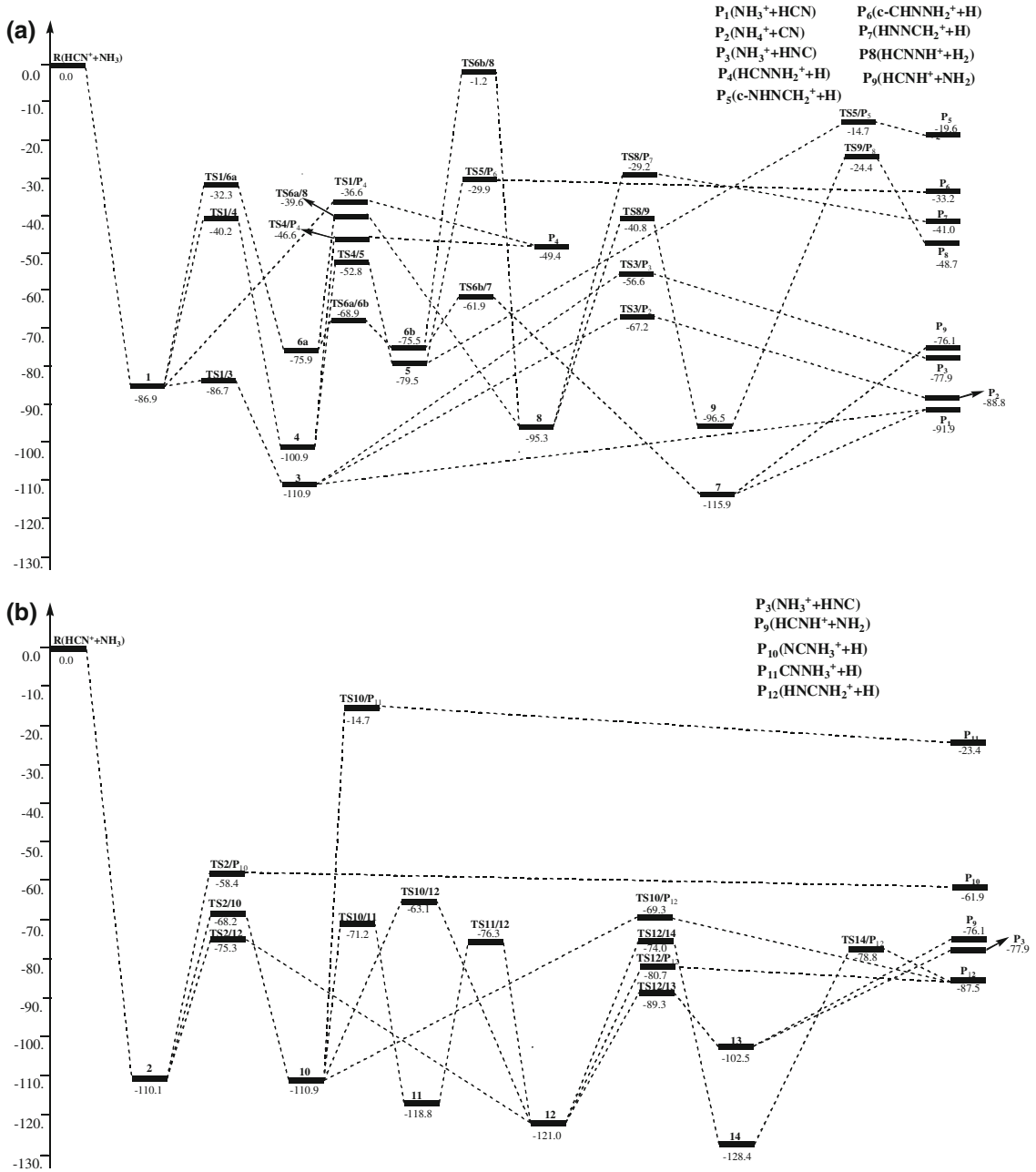

Fig. 4 The potential energy surface (PES) of the reaction channels for the $HCN^{+}+NH_3$ reaction. *E*rel are the relative energies (kcal/mol)

$\mathbf{P_{11}}(CNNH_3^{+}+H)$, and $\mathbf{P_{12}}(HNCNH_2^{+}+H)$ are obtained via successive isomerization and dissociation pathways. In the following discussion, we focus on the formation pathways of these five products.

$$\mathbf{P_3}\left(\mathbf{NH_3^+ + HNC}\right) \quad (1)$$

From Fig. 4b, we find that three pathways are possible to yield $\mathbf{P_3}$ which can be depicted as:

Path $\mathbf{P_3}$ (1) R → 2 → 12 → 13 → $\mathbf{P_3}$

Path $\mathbf{P_3}$ (2) R → 2 → 10 → 12 → 13 → $\mathbf{P_3}$

Path $\mathbf{P_3}$ (3) R → 2 → 10 → 11 → 12 → 13 → $\mathbf{P_3}$

In **path $\mathbf{P_3}$(1)**, the initial adduct **2** $NCHNH_3^{+}$ undergoes 1,3-H-shift to generate **12** $HNCHNH_2^{+}$ followed by concerted C–N cleavage and 2,3-H-shift lead to the weakly bound complex **13** $HNC\cdots HNH_2^{+}$. Finally **13** can directly dissociate to $\mathbf{P_3}$. Alternatively, **2** can undergo 1,2-H-shift to yield **10** $HNCNH_3^{+}$. Subsequently, **10** can take either 2,3-H-shift to generate **12** as in **path $\mathbf{P_3}$(2)**, or successive 1,3-H and 1,2-H-shift to generate **11** *v*-$NH_2CNH_2^{+}$, then to **12** as in **path $\mathbf{P_3}$(3)**. The fate of

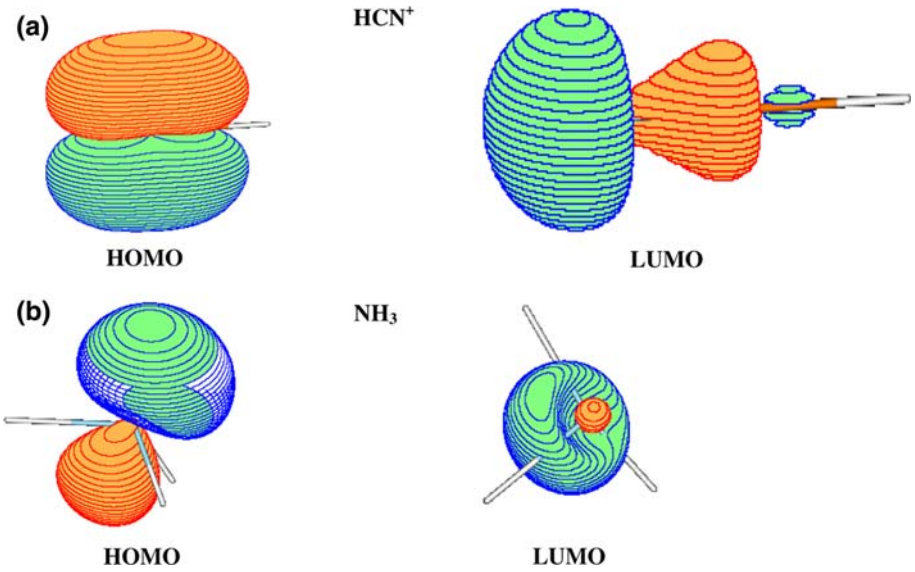

Fig. 5 HOMO and LUMO orbital pictures of reactant

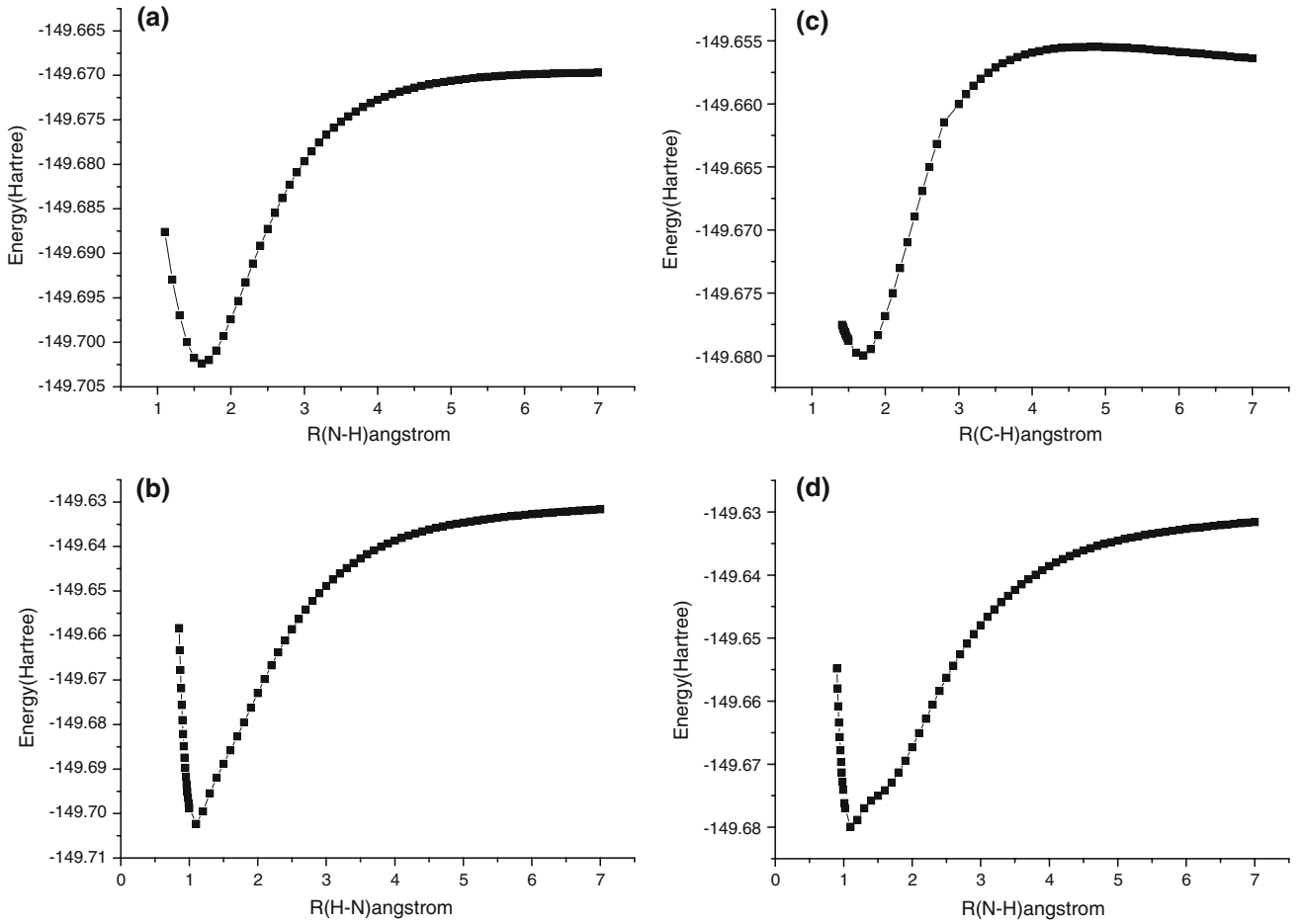

Fig. 6 **a** Dissociation curve of 7-P_1 computed at the B3LYP/6-311G(d,p) level. **b** Dissociation curve of 7-P_9 computed at the B3LYP/6-311G(d,p) level. **c** Dissociation curve of 13-P_3 computed at the B3LYP/6-311G(d,p) level. **d** Dissociation curve of 13-P_9 computed at the B3LYP/6-311G(d,p) level

12 is the same as that in **path P_3(1)**. Note that **13→P_3** conversion is a barrierless process, the dissociation curve of **13** is plotted in Fig. 6c.

Clearly, **path P_3(1)** is relatively simple than the latter two paths, then we expect **path P_3(1)** is competitive than **path P_3(2–3)**. Now, let us compare the feasibility of **path P_3(1)** with **path P_3 (R→1→3→P_3)** which has been discussed previously. One high barrier 54.3 (**3→P_3**) kcal/mol is involved in **path P_3**, while two moderate barriers are involved in **path P_3(1)**, which are 34.8 and 31.7 kcal/mol for **2→12** and **12→13** conversions, respectively. In addition, the transition state **TS3/P_3** (−56.6) in **path P_3** is much higher than **TS2/12** (−75.3) and **TS12/13** (−89.3) in **path P_3(1)**. In view of these factors, we expect **path P_3(1)** should be the favorite channel to form **P_3**.

P_9 (**$HCNH^+ + NH_2$**) (2)

From Fig. 4b, we find that three pathways are associated with the formation of **P_9**. They can be written as:

Path P_9 (1) R → 2 → 12 → 13 → P_9

Path P_9 (2) R → 2 → 10 → 12 → 13 → P_9

Path P_9 (3) R → 2 → 10 → 11 → 12 → 13 → P_9

The formation pathway of **13** HNC···HNH_2^+ has been discussed previously. Then, **13** can directly dissociate to **P_9** without any encounter barrier. To confirm **13→P_9** is a barrierless process, we calculate the pointwise potential curve at the B3LYP/6-311G(d,p) level. The dissociation curve of **13** is shown in Fig. 6d.

Obviously, **path P_9(1)** is simpler than **path P_9(2–3)**, thus **path P_9(1)** should be the most feasible channel to form **P_9**.

P_{10}(**$NCNH_3^+ + H$**)**and** **P_{11}**(**$CNNH_3^+ + H$**) (3)

Only one possible pathway is associated with the formation of **P_{10}** ($NCNH_3^+ + H$) and **P_{11}** ($CNNH_3^+ + H$), they can be written as:

Path P_{10} R → 2 → P_{10}

Path P_{11} R → 2 → 10 → P_{11}

In **path P_{10}**, **2** $NCHNH_3^+$ undergoes C–H bond rupture to form **P_{10}** with the energy barrier of 51.7 kcal/mol. In **path P_{11}**, **2** takes 1,2-H-shift to form **10** $HNCNH_3^+$. Then **10** undergoes a concerted C–N bond rupture, N–N bond formation and H-elimination process lead to **P_{11}**. The energy barriers for **2→10** and **10→P_{11}** conversions are 41.9 and 96.2 kcal/mol, respectively.

P_{12}(**$HNNCH_2^+ + H$**) (4)

For product **P_{12}**, six pathways are energetically possible as follows:

Path P_2 (1) R → 2 → 12 → P_{12}

Path P_{12} (2) R → 2 → 10 → 12 → P_{12}

Path P_{12} (3) R → 2 → 10 → 11 → 12 → P_{12}

Path P_{12} (4) R → 2 → 12 → 14 → P_{12}

Path P_{12} (5) R → 2 → 10 → 12 → 14 → P_{12}

Path P_{12} (6) R → 2 → 10 → 11 → 12 → 14 → P_{12}

The formation of **12** $HNCHNH_2^+$ is the same as that in **path P_3(1)**. Subsequently, **12** undergoes either C–H bond rupture to form **P_{12}** as in **path P_{12} (1–3)**, or successive 1,2-H-shift and N–H bond dissociation to generate **14** *p*-$NH_2CNH_2^+$, then to **P_{12}** as in **path P_{12} (4–6)**. The barriers for the steps of **12→P_{12}**, **12→14**, and **14→P_{12}** are 40.3, 47.0 and 49.6 kcal/mol, respectively.

By comparison, we find that **path P_{12} (1–3)** are simpler than **path P_{12} (4–6)**, thus the former three pathways should be competitive than the latter three pathways. With respect to the former three pathways, **path P_{12} (1)** is the simplest one, it should be the favorite path to form **P_{12}**.

4 Reaction mechanism

In the previous section, we have obtained twelve kinds of dissociation products **P_1**($NH_3^+ + HCN$), **P_2**($NH_4^+ + CN$), **P_3**($NH_3^+ + HNC$), **P_4**($HCNNH_2^+ + H$), **P_5**(c-$NHNCH_2^+ + H$), **P_6**(c-$CHNNH_2^+ + H$), **P_7**($HNNCH_2^+ + H$), **P_8**($HCNNH^+ + H_2$), **P_9** ($HCNH^+ + NH_2$), **P_{10}**($NCNH_3^+ + H$), **P_{11}**($CNNH_3^+ + H$), and **P_{12}**($HNCNH_2^+ + H$). For easier discussion, the most feasible formation pathways for these twelve products are listed again.

Path P_1(1) R → 1 → 3 → P_1

Path P_2 R → 1 → 3 → P_2

Path P_3(1) R → 2 → 12 → 13 → P_3

Path P_4(1) R → 1 → P_4

Path P_5 R → 1 → 4 → 5 → P_5

Path P_6 R → 1 → 4 → 5 → P_6

Path P_7(1) R → 1 → 6a → 8 → P_7

Path P_8(1) R → 1 → 6a → 8 → 9 → P_8

Path P_9(1) R → 2 → 12 → 13 → P_9

Path P_{10} R → 2 → P_{10}

Path P_{11} R → 2 → 10 → P_{11}

Path P_{12}(1) R → 2 → 12 → P_{12}

The rate-determining transition state **TS1/P_4**(−36.6) in **path P_4(1)**, **TS5/P_5**(−14.7) in **path P_4**, **TS5/P_6**(−29.9) in **path P_6**, **TS8/P_7**(−29.2) in **path P_7(1)**, and **TS9/P_8**(−24.4) in **path P_8(1)** and **TS10/P_{11}**(−14.7) in **path P_{11}** lies significantly high, which makes them kinetically

unfeasible. Therefore, products **P_4**, **P_5**, **P_6**, **P_7**, **P_8** and **P_{11}** may unlikely be detected in experiment.

Now, let us compare the feasibility of the remaining six products **P_1**, **P_2**, **P_3**, **P_9**, **P_{10}**, and **P_{12}**. First, because **TS2/P_{10}**(−58.4) in **path P_{10}** lies much higher than **TS1/3**(−86.7) in **path P_1(1)**, **TS3/P_2**(−67.2) in **path P_2**, and **TS2/12**(−75.3) in **path P_3(1)**, **path P_9(1)**, and **path P_{12}(1)**. **Path P_{10}** should be the least competitive channel. Second, the relative energy of **TS12/P_{12}**(−80.7) is higher than that of **TS12/13**(−89.3) in both **path P_3(1)** and **path P_9(2)**, which makes **path P_{12}(1)** less competitive than **path P_3(2)** and **path P_9(2)**. **Path P_3(2)** and **path P_9(1)** may compete with each other since the relative energies of **P_3** and **P_9** are very close within 1.8 kcal/mol. So, we expect that these two paths may have comparable contribution to the title reaction. Third, as shown in Fig. 4, **P_1** lie much lower than **TS3/P_2** and **P_2** in **path P_2**. This makes **P_1** the dominant product from **3**, and thus **P_2** may have undetected yield.

Reflected in the final products distributions, a total of six kinds of products **P_1**(NH_3^+ + HCN), **P_2**(NH_4^+ + CN), **P_3**(NH_3^+ + HNC), **P_9**($HCNH^+$ + NH_2), **P_{10}**($NCNH_3^+$ + H), and **P_{12}**($HNCNH_2^+$ + H) may be observed. Among, **P_1** should be the dominant product with largest yield, **P_3** and **P_9** may be the second feasible products with comparable yields. **P_{12}** may be the third feasible product. **P_2** and **P_{10}** may be the least feasible products with almost negligible yields.

Of course, for the present reaction system, it is desirable to make kinetic studies. However, such calculations are beyond the scope of the present article, and not considered further.

5 Comparison with experiments

For $HCN^+ + NH_3$ reaction, only one experimental study has been carried out at room temperature [17]. The measured large rate constant of 2.8×10^{-9} cm^3 s^{-1} at 300 K can be explained by the fact that the title reaction is a barrierless association, isomerization and dissociation process. Furthermore, McEwan et al. [17] obtained three products $NH_3^+ + HCN$, $NH_4^+ + CN$ and $HCNH^+ + NH_2$ with the respective branching ratios of 0.6, 0.05 and 0.3. $NH_3^+ + HCN$ corresponds to **P_1** in our theoretical studies, and the distribution is the highest in all products. $HCNH^+ + NH_2$ corresponds to **P_9** which also has an upper branching ratio. $NH_4^+ + CN$ can be found as a negligible product **P_2** in our results. In these aspects, our theoretical results are in nice agreement with previous experimental studies. On the other hand, we predict another product **P_3** (NH_3^++HNC) which was completely ignored by McEwan et al. Based on our results, **P_3** may have the same contribution as **P_9**($HCNH^+ + NH_2$). Therefore, further experimental reinvestigation of the title reaction is desirable.

6 Reliability assessment

For the species involved in the most feasible formation pathways of each products, we performed additional single-point energy calculations at the G3B3 level using the B3LYP/6-311G(d,p)-optimized geometries and scaled B3LYP/6-311G(d,p)-zero-point energies. The relative energies of these 31 species at the CCSD(T)/6-311++G(3df,2pd)//B3LYP/6-311G(d,p) + ZPVE and G3B3//B3LYP/6-311G(d,p) levels are very close to each other with the largest deviation 2.8 kcal/mol of **TS12/P_{12}**. Thus, we expect that the CCSD(T)/6-311++G(3df,2pd)//B3LYP/6-311G(d,p) + ZPVE method can provide reliable mechanistic information for the $HCN^+ + NH_3$ reaction.

7 Conclusion

The B3LYP and CCSD(T) methods are used to explore the potential energy surface of the ion–molecule reaction of HCN^+ with NH_3, which has never been studied theoretically. The association between HCN^+ and NH_3 is found to be barrierless process forming two adducts, **1** $HCNNH_3^+$, and **2** $NCHNH_3^+$. Subsequently, **1** and **2** can take further changes which lead to various products. We predict that six kinds of dissociation products may be observed. Among them, **P_1**(NH_3^+ + HCN) is the most competitive product with predominant abundance. **P_3** (NH_3^+ + HNC) and **P_9** ($HCNH^+$ + NH_2) are the less feasible products with comparable quantities, followed by the least possible **P_{12}**($HNCNH_2^+$ + H). **P_2**(NH_4^+ + CN) and **P_{10}**($NCNH_3^+$ + H) may have negligible yields. The barrierless nature of the title reaction indicates that title reaction may have a potential relevance in Titan's atmosphere.

Acknowledgments This work is supported by the National Natural Science Foundation of China (Nos. 20773048).

References

1. Bauer SJ (1987) Adv Space Res 7:65
2. Cravens TE, Robertson IP, Waite JH, Yelle RV, Kasprzak WT, Keller CN, Ledvina SA, Niemann HB, Luhmann JG, McNutt RL, Ip WH, DeLaHaye V, Mueller-Wodarg I, Wahlund JE, Anicich VG, Vuitton V (2006) Geophys Res Lett 33:07105
3. Fulchignoni M, Ferri F, Angrilli F, Ball AJ, Bar-Nun A, Barucci MA, Bettanini C, Bianchini G, Borucki W, Colombatti G, Coradini M, Coustenis A, Debei S, Falkner P, Fanti G, Flamini E, Gaborit V, Grard R, Hamelin M, Harri MA, Hathi B, Jernej I, Leese MR, Lehto A, LionStoppato PF, López-Moreno JJ, Mäkinen T, McDonnell JAM, McKay CP, Molina-Cuberos G, Neubauer FM, Pirronello V, Rodrigo R, Saggin B, Schwingenschuh K, Seiff A, Simões F, Svedhem H, Tokano T, Towner MC, Trautner R, Withers P, Zarnecki JC (2006) Nature 438:785

4. Vuitton V, Yelle RV, McEwan MJ (2007) Icarus 191:722
5. Vuitton V, Yelle RV, Anicich VG (2006) Astrophys J 647:175
6. Vuitton V, Doussin JF, Bénilan Y, Raulin F, Ganeau MC (2006) Icarus 185:287
7. Broadfoot AL, Sandel BR, Shemansky DE, Holberg JB, Smith GR, Strobel DF, McConnell JC, Kumar S, Hunten DM, Atreya SK, Donahue TM, Moos HW, Bertaux JL, Blamont JE, Pomphrey RB, Linick S (1981) Science 212:206
8. Hanel R, Conrath B, Flasar FM, Kunde V, Maguire W, Pearl J, Pirraglia J, Samuelson R, Herath L, Allison M, Cruikshank D, Gautier D, Gierasch P, Horn L, Koppany R, Ponnamperuma C (1980) Science 212:192
9. Samuelson R, Nath N, Borysow A (1997) Planet Space Sci 45:959
10. Yung YL, Allen M, Pinto JP (1984) Appl J Suppl 55:465
11. Toublanc D, Parisot JP, Brillet J, Gautier D, Raulin F, McKay CP (1995) Icarus 113:2
12. Fox JL, Yelle RV (1997) Geophys Res Lett 24:2179
13. Keller CN, Anicich VG, Craven TE (1998) Planet Space Sci 46:1157
14. Banaskiewicz M, Lara ML, Rodrigo R, López-Moreno JJ, Molina-Cuberos GJ (2000) Icarus 147:386
15. Wahlund JE, Bostro MR, Gustafsson G, Gurnett DA, Kurth WS, Pedersen A, Averkamp TF, Hospodarsky GB, Personn AM, Canu P, Neubauer FM, Dougherty MK, Eriksson AI, Morooka MW, Gill R, André M, Eliasson L, Müller-Wodarg I (2005) Science 308:986
16. Lilensten J, Simon C, Witasse O, Dutuit O, Thissen R, Alcaraz C (2005) Icarus 174:285
17. McEwan MJ, Anicich VG, Huntress MT (1981) Int J Mass Spectrom Ion Phys 37:273
18. Vacher JR, Le Duc E, Fitaire M (1997) Planet Space Sci 45:1407
19. Mcewan MJ, Scott GBI, Anicich VG (1998) Int J Mass Spectrom Ion Proc 172:209
20. Vacher JR, Le Duc E, Fitaire M (2000) Planet Space Sci 48:237
21. Anicich VG, Milligan DB, Fairley DA, McEwan MJ (2000) Icarus 146:118
22. Milligan DB, Freeman CG, Maclagan RGAR, McEwan MJ, Wilson PF, Anicich VG (2001) J Am Soc Mass Spectrom 12:557
23. Anicich VG, McEwan MJ (2001) Icarus 154:522
24. Carrasco N, Dutuit O, Thissen R, Banaszkiewicz M, Pernot P (2007) Planet Space Sci 55:141
25. Frisch MJ, Trucks GW, Schlegel HB, Scusera GE, Robb MA, Cheeseman JR, Zakrzewski VG, Montgomery JA Jr, Stratmann RE, Burant JC, Dapprich S, Millam JM, Daniels AD, Kudin KN, Strain MC, Farkas O, Tomasi J, Barone V, Cossi M, Cammi R, Mennucci B, Pomelli C, Adamo C, Clifford S, Ochterski J, Petersson GA, Ayala PY, Cui Q, Morokuma K, Malick DK, Rabuck AD, Raghavachari K, Foresman JB, Cioslowski J, Ortiz JV, Stefanov BB, Liu G, Liashenko A, Piskorz P, Komaromi I, Gomperts R, Martin RL, Fox DJ, Keith T, Al-Laham MA, Peng CY, Nanayakkara A, Gonzalez C, Challacombe M, Gill PMW, Johnson B, Chen W, Wong MW, Andres JL, Gonzalez C, Head-Gordon M, Replogle ES, Pople JA (1998) Gaussian 98, Revision A.6. Gaussian Inc., Pittsburgh, PA